Mon. Not. R. Astron. Soc. **380,** 949–962 (2007) doi:10.1111/j.1365-2966.2007.12177.x

Star formation and stellar populations across nuclear rings in galaxies

M. Sarzi,[1⋆] E. L. Allard,[1] J. H. Knapen[1,2] and L. M. Mazzuca[3]

[1]*Centre for Astrophysics Research, University of Hertfordshire, College Lane, Hatfield, Herts AL10 9AB*
[2]*Instituto de Astrofísica de Canarias, E-38200 La Laguna, Spain*
[3]*NASA Goddard Space Flight Center, Code 441, Greenbelt, MD 20771, USA*

Accepted 2007 July 2. Received 2007 June 22; in original form 2007 May 11

ABSTRACT

We present a study of the optical spectra of a sample of eight star-forming nuclear rings and the nuclei of their host galaxies. The spectra were obtained with the Intermediate dispersion Spectrograph and Imaging System spectrograph on the William Herschel Telescope and cover a wide range in wavelength, enabling the measurement of several stellar absorption features and gas emission lines.

We compared the strength of the absorption lines to a variety of population synthesis models for the star formation history in the nuclear rings, including also the contribution of the older bulge and disc stellar components. In agreement with our previous investigation of the nuclear ring of NGC 4321, which was based on a more restricted number of line-strength indices, we find that the stars in our sample of nuclear rings have most likely formed over a prolonged period of time characterized by episodic bursts of star formation activity. Constant star formation is firmly ruled out by the present data, whereas a one-off formation event is an unlikely explanation for a common galactic component such as nuclear rings. The nuclear rings of NGC 4314 and NGC 7217 have distinct line-strength properties that set them apart from the rest of our sample, which are due to a larger contribution of bulge star in the observed spectra and, in the case of NGC 4314, to a younger stellar population in the ring.

We have used emission-line measurements to constrain the physical conditions of the ionized gas within the rings, using the ratio of the [S II]λλ6716, 6731 lines to estimate the density of the gas, and photoionization model grids within specific diagnostic diagrams to derive metallicity. We find that emission in all nuclear rings originates from H II regions with electron densities typical for these kinds of objects, and that the rings are characterized by values for the gas metallicity ranging from slightly below to just above solar. We have also studied the spectra of the nuclei of our sample galaxies, all of which display emission lines. Consistent with previous studies for the nuclear activity and stellar populations, the majority of our nuclei appear to be dominated by old stellar populations and by Low-Ionization Nuclear Emission Region like emission.

As 20 per cent of nearby spiral galaxies host nuclear rings that are presently forming massive stars, our finding of an episodic star formation history in nuclear rings implies that a significant population remains to be identified of young nuclear rings that are not presently in a massive star formation phase. Nuclear rings may thus be a much more common galactic component than presently known.

Key words: H II regions – galaxies: ISM – galaxies: nuclei – galaxies: spiral – galaxies: star clusters – galaxies: stellar content.

1 INTRODUCTION

Star-forming nuclear rings occur in approximately 20 per cent of spiral galaxies (Knapen 2005). Generally, they are sites of intense active star formation, containing a mixture of gas, dust and young stars. This is deduced from their blue colours, bright hydrogen emission lines in optical and infrared (IR), enhanced radio continuum emission, and overall patchy appearance (Arsenault et al. 1988; Pogge 1989; García-Barreto et al. 1991; Benedict et al. 1992; Knapen et al. 1995a,b; Benedict, Smith & Kenney 1996; Jogee et al. 2002; Allard, Peletier & Knapen 2005; Mazzuca et al. 2006, 2007). Additionally,

⋆E-mail: m.sarzi@herts.ac.uk

red nuclear dust rings have been identified (e.g. Buta & Crocker 1991; Vila-Vilaró et al. 1995; Wozniak et al. 1995), as well as so-called 'fossil rings', which are dust-free and composed entirely of stars, and virtually indistinguishable from the surrounding stellar population (Erwin, Vega Beltran & Beckman 2001; Erwin & Sparke 2002).

The vast majority of nuclear rings appear in barred galaxies (Knapen 2005), where the bar has the ability to channel gas from the disc towards the nucleus (e.g. Huntley, Sanders & Roberts 1978; Sanders & Tubbs 1980; Simkin, Su & Schwarz 1980; van Albada & Roberts 1981; Schwarz 1984; Combes & Gerin 1985; Shlosman, Begelman & Frank 1990; Athanassoula 1992; Knapen et al. 1995a,b). During this process, the radial inflow of gas is slowed down near the location of the inner Lindblad resonances (ILRs), which allows for the accumulation of gas and which can, ultimately, lead to a star-forming ring (Combes & Gerin 1985; Shlosman, Frank & Begelman 1989; Wada & Habe 1992; Heller & Shlosman 1994; Knapen et al. 1995a,b; Fathi et al. 2005). In a few cases, two of which will be discussed in this paper, nuclear rings occur in host galaxies without an obvious kpc-scale bar. The formation of such rings may be related to the presence of a weak oval distortion (Buta et al. 1995), to a dissolved bar (Verdes-Montenegro, Bosma & Athanassoula 1995), to the tidal effects of a companion galaxy (Combes 1988), or to a recent minor merger (Knapen et al. 2004; Mazzuca et al. 2006).

At least two-thirds of all spirals are barred (de Vaucouleurs 1963; Sellwood & Wilkinson 1993; Eskridge et al. 2000; Knapen, Shlosman & Peletier 2000; Grosbøl, Patsis & Pompei 2004). Jogee et al. (2004), Elmegreen, Elmegreen & Hirst (2004) and Zheng et al. (2005) showed that the bar fraction is roughly constant out to $z \approx 1$, indicating that bars are long-lived phenomena. Since gas is readily available in the disc, nuclear rings may continue to form stars as long as the bar continues to provide an inflow of fresh material. Even with continued inflow at the rates thought to be supplied by a typical bar (around a solar mass per year), the high star formation rates within the rings can exhaust the gas relatively quickly (Elmegreen et al. 1998), effectively turning off the star formation. As more gas is supplied to the ring the density will gradually increase, until star formation is initiated again. The moderate inflow rates and observed elevated star formation rates thus indicate that the star-forming process in nuclear rings may cycle through active and quiescent periods. The fraction of galaxies with nuclear rings may thus be significantly larger than the fraction of rings seen to be forming massive stars at present (which is around 20 per cent; Knapen 2005).

At the present time, however, observational confirmation of this longevity of nuclear rings is still limited. As such, the effect nuclear rings may have on the evolution of their host galaxies is unclear. The ages of individual star-forming regions, sometimes referred to as hotspots, in nuclear rings have been studied using a variety of techniques, almost all based on the use of optical or near-IR recombination emission lines via imaging or spectroscopy (e.g. Engelbracht et al. 1998; Puxley & Brand 1999; Ryder & Knapen 1999; Kotilainen et al. 2000; Alonso-Herrero, Ryder & Knapen 2001; Ryder, Knapen & Takamiya 2001; Díaz-Santos et al. 2007; Mazzuca et al. 2007). These lines trace primarily very young and massive stars, and as a consequence the ages derived using these techniques are usually below 10 Myr, or otherwise very sensitive to assumptions on the star formation history. Broad-band colours have also been used to estimate the age of the stellar population in circumnuclear rings (e.g. Kotilainen et al. 2000; Harris et al. 2001). Such measurements, however, are affected by reddening and degeneracies between age and metallicities, and even in the case of near-IR data, where the impact of dust is mitigated, the interpretation of colour–colour diagrams is complicated by the fact that populations of very different ages have very similar colours (see e.g. the models of Maraston 2005). In contrast, the technique employed in this paper, which is based on the strength of several stellar absorption lines, is sensitive to a much larger range of intermediate ages, is unaffected by reddening and is known to break the age–metallicity degeneracy that limits broad-band estimations (Worthey 1994).

Based on such an interpretation of line-strength indices, in Allard et al. (2006, hereafter Paper I), we presented strong evidence that the nuclear ring in NGC 4321 (Messier 100) is indeed long lived, though forming stars episodically in a rapid succession of bursts rather than continuously. Due to the limited wavelength range of the data we used, we could, however, not completely rule out the possibility that the rings are transient objects. With our long-slit data (presented in this paper), we cover a much wider wavelength range and aim to confirm the nature of the nuclear ring in NGC 4321, as well as seven other well-known rings, with the goal of generalizing the star formation activity pattern and evolutionary past within nuclear rings.

In this paper, we study the star formation histories of eight nuclear rings, by extracting information from long-slit Intermediate dispersion Spectrograph and Imaging System (ISIS) spectra over a wide range in wavelength, analysing both the stellar and the gaseous contributions to the spectra. For each nuclear ring, we have one to three spectrograph slit position angles (PAs) each of which bisects the nucleus and the ring, yielding data on two to six H II regions, referred to as hotspots, for each ring (see Fig. 1). Studying the stellar absorption and gas emission lines will thus allow us to determine the physical parameters and complex star formation properties of these rings.

This paper is structured as follows. Section 2 details the observations and data reduction, and Section 3 describes the analysis of the data. The results of the stellar absorption-line analysis are presented in Section 4, and the analysis of the emission lines is presented in Section 5. Finally, we present our discussions and conclusions in Sections 6 and 7.

2 OBSERVATIONS AND DATA REDUCTION

The observed galaxies were chosen from the Hα sample of Knapen et al. (2006), and are all known to possess strong Hα-emitting nuclear rings. Our sample consists of six galaxies with moderate to strong bars, and two galaxies that appear to be unbarred, at least at first glance. These two unbarred galaxies, NGC 7217 and NGC 7742, are both known to have counter-rotating subsystems in their central regions (Merrifield & Kuijken 1994; Sil'chenko & Afanasiev 2000; de Zeeuw et al. 2002), which may suggest a history of interaction. Some global parameters for the eight galaxies are listed in Table 1. The ISIS spectrograph on the William Herschel Telescope (WHT) on La Palma was used to observe five galaxies on 2001 April 29 and 30. An additional three galaxies were observed on the 2005 October 5 using the same instrument. Details of the observations, including spectrograph slit PAs for each galaxy, are listed in Table 2. Hα images of all the nuclear rings and the slit PAs used in each case are shown in Fig. 1.

The slit was always positioned so it targetted the nucleus and at least one bright hotspot in the ring. A slit width of 1 arcsec was used. We operated ISIS with a dichroic, which allows simultaneous observations with a red and a blue arm, covering wavelength ranges of 3500–5700 Å and 5900–8900 Å, respectively. The R158B

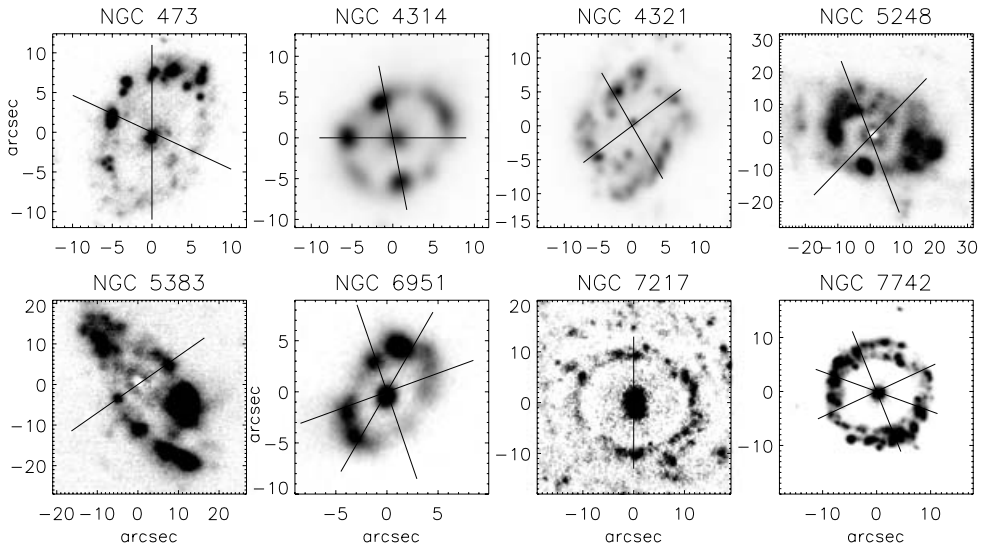

Figure 1. Hα continuum-subtracted images of the nuclear rings in the sample (data from Knapen et al. 2006). The black lines show the slit positions of the spectrograph. The north is up, and the east is to the left-hand side.

Table 1. Global parameters of the observed galaxies. Tabulated are the NGC number, the morphological type from NED, the nuclear activity class from Ho et al. (1997), and the distance D and the physical scales both from Knapen et al. (2006).

Galaxy	Type	Activity	D (Mpc)	Scale (pc arcsec^{-1})
NGC 473	SAB(r)0/a		29.8	144.5
NGC 4314	SB(rs)a	L2	9.7	47.0
NGC 4321	SAB(s)bc	T2	16.8	81.4
NGC 5248	(R)SB(rs)bc	H	22.7	110.1
NGC 5383	(R')SB(rs)b	H	37.8	183.3
NGC 6951	SAB(rs)bc	S2	24.1	116.8
NGC 7217	(R)SA(r)ab	L2	16.0	77.6
NGC 7742	SA(r)b	T2/L2	22.2	107.6

Table 2. Observing run details. Given are the galaxy name, the date of the observations, the exposure times, and the PAs of the spectrograph slit, measured north over east.

Galaxy	Date	Exposure times (s)	PA (°)
NGC 473	05/10/05	3 × 1200	0
	05/10/05	3 × 1200	65
NGC 4314	29/04/01	2 × 1800	11
	29/04/01	3 × 1800	90
NGC 4321	30/04/01	3 × 1200	127
	30/04/01	2 × 1200	210
NGC 5248	29/04/01	2 × 1800	22
	29/04/01	1 × 1800	136
NGC 5383	30/04/01	3 × 1200	125
NGC 6951	29/04/01	2 × 1800	150
	05/10/05	3 × 1200	19
	05/10/05	3 × 1200	110
NGC 7217	05/10/05	3 × 1200	0
NGC 7742	05/10/05	3 × 1200	22
	05/10/05	3 × 1200	70
	05/10/05	3 × 1200	115

grating was used for the blue arm, providing 1.62 Å pixel^{-1} and 0.2 arcsec pixel^{-1} scales with the EEV12 detector. For the initial observing run the R158R grating was used with the TEK4 detector on the red arm, which gave 2.90 Å pixel^{-1} and 0.36 arcsec pixel^{-1} scales. For the second observing run the TEK4 detector was no longer in operation, and the red MARCONI detector was used, which provides similar spatial and spectral scales to the blue EEV12 detector. The instrumental resolution was 180 km s^{-1} (σ = 6.8 Å) for the blue, and 115 km s^{-1} (σ = 5.8 Å) for the red arm. Standard CuAr+CuNe calibration lamp exposures were taken before and after each science exposure, along with a number of spectroscopic standard star observations for flux calibration.

Although the spectrograph slit passed through two hotspots in NGC 5383, neither had high enough signal-to-noise ratio (S/N) to be useful. The two extracted spectra were instead combined. Additionally, the two hotspots measured in NGC 7217 had a sufficient S/N in their stellar continuum, but not in their gas emission lines. The two spectra were thus averaged for the emission-line measurements but not for the stellar index measurements.

The spectra were reduced within the IRAF package using standard methods. The data were first bias- and overscan-corrected, before trimming and flat-fielding. A cosmic-ray removal algorithm was applied next. The separate exposures were then checked for offsets in positions between adjacent exposures, shifted if necessary, and combined. The spatial regions along the slit containing the hotspots and the nucleus were extracted and median-combined to produce a one-dimensional spectrum. CuNe+CuAr lamp exposures were used for wavelength calibration, with typical errors of 0.1 Å. The spectra were traced to align the dispersion and spatial axes with the rows and columns of the CCD array. To remove the background sky contribution, regions at the outer edges of the slit were averaged to produce a one-dimensional spectrum which was subtracted from every row in the image. The spectra were flux-calibrated to an absolute scale with units of erg cm^{-2} s^{-1} Å^{-1}, with typical errors of 30 per cent. A number of atmospheric absorption and emission lines are found towards the end of the red spectral range, which could not be removed sufficiently in all cases. Consequently, the red spectra were trimmed to give a wavelength coverage of 5800–6800 Å, which includes the important emission lines of Hα, [N II] and [S II]. Fig. 2 shows two

examples of blue spectra subtending the nucleus and one of the ring hotspots of NGC 4314.

3 DATA ANALYSIS

The stellar and gaseous contributions to the spectra were separated using the direct fitting method described in Sarzi et al. (2006).[1] We modelled the stellar continuum with linear combinations of synthetic spectral templates from Bruzual & Charlot (2003), adopting the same library used by Tremonti et al. (2004). This includes 13 template spectra for each of the three metallicities $Z = 0.004$, 0.02 and 0.05, corresponding to 10 instantaneous-burst models with ages from 5 Myr to 11 Gyr, a constant star formation model with an age of 6 Gyr, and two models with exponentially declining star formation histories with ages of 9 and 12 Gyr.

The spectral regions affected by nebular emission are not excluded from the fitting process. Instead, the emission lines are treated as Gaussian templates and fitted simultaneously with the stellar templates to the observed spectra. This has the advantage of maximizing the spectral information available to the fitting algorithm.

As the blue and red spectra have different spectral resolutions, they could not be fitted simultaneously. The blue spectra cover a much wider wavelength range than the red, and contain a large number of stellar absorption features that help constrain the mix of stellar templates. We therefore fit the blue spectra first, and use the resulting optimal combination of templates to match the red spectra, allowing only for a different velocity broadening. The fits to the blue spectra include reddening due to foreground interstellar dust, both in the Milky Way and in the sample galaxies, and due to dust in the emission-line regions. The latter affects only the fluxes of the emission-line templates, and is constrained by the expected and observed decrement of the Balmer lines. Setting physically motivated limits on the intensity of the emission from high-order Balmer lines is of particular importance to ensure that the strength of the corresponding absorption features remains unbiased, and will thus not affect our stellar population analysis. A similar methodology was applied also by Shields et al. (2007). The derived weights of the stellar spectra that define the optimal template are used to reconstruct an unconvolved optimal template, which is free from the effects of velocity broadening. This unconvolved optimal template is used to measure the absorption-line strengths.

Owing mostly to the varied nature of the Tremonti et al. library, the template-fitting procedure yields excellent results in matching the spectra extracted from both the ring and the nuclear apertures in all but two cases. The two exceptions are the blue spectra of NGC 6951 at PA $= 110^\circ$ and 150°. In the following, we will ignore the line-strength measurements obtained from these spectra. Since the nebular emission is sufficiently strong to allow robust estimates of the emission-line fluxes, even where the fit to the stellar continuum is poor, we will use the emission-line results derived from these two spectra.

3.1 Line strengths and indices

Stellar absorption lines provide information on the stellar content of the rings. The strength of an absorption-line index is determined by the difference between the absorption line and the continuum level. An index is typically defined by a wavelength range that contains the feature and two wavelength ranges to either side that provide an estimate of the red and blue continuum levels. The mid-points of the continuum passbands are fitted by a linear relation, and the difference between this and the absorption feature provides the index value. The latter is sensitive to the shape of the continuum, the spectral resolution, and the velocity dispersion of the object. All these factors must be taken into account before one set of measurements can be compared with another. The Lick/IDS system (Worthey 1994) is commonly used to compare measurements from different observations. For the data used in this paper, however, we are mostly concerned with comparing our indices with model predictions, and for this we need only to ensure that our indices are measured in the same way as they are in the models. By construction, the model predictions come from model spectra with identical resolution to our optimal templates, so it is appropriate to compare them. The line strengths were measured using INDEXF, a C++ program written by N. Cardiel,[2] with the Lick/IDS wavelength definitions (but not calibrated to the Lick/IDS system).

3.2 Uncertainties

The uncertainties in the index measurements are largely determined by the quality of the optimal template fit to the observed galaxy continuum. Kuntschner et al. (2006) describe the errors associated with our emission and absorption-line fitting method and subsequent measurements of line strengths. From a detailed analysis, they find a constant error budget of 0.1 Å from the continuum fitting process, which we adopt for all the stellar absorption-line indices presented here. With regard to the emission-line fluxes, Sarzi et al. (2006) find from simulations that the uncertainties associated with flux measurements scale with the level of fluctuations in the residuals of the fit to the spectrum. We convert such residual-noise levels into an estimate for the emission-line flux errors, adopting as an error for each line the flux of a Gaussian with amplitude equal to the residual-noise level and width equal to the width of the emission line in question. Considering the weaker lines that will enter our emission-line analysis, Hβ and [O III], these come on average with 3 and 26 per cent uncertainties, respectively, which translate to a typical error of 0.12 on the logarithm of the [O III]/Hβ line ratio. Errors on line ratios based on the stronger emission lines in our red spectra (e.g. Hα, [N II], [S II]) will be smaller than that.

4 STELLAR ABSORPTION-LINE DIAGNOSTICS: THE STAR FORMATION HISTORY

4.1 Index–index diagrams and single starburst models

To probe the properties of unresolved stellar populations, several combinations of absorption-line strength indices are traditionally used to separate age and metallicity effects, comparing the measured values to predictions for stellar populations that were born in an instantaneous burst of star formation and for a single metallicity. Using such single starburst population (SSP) models from Bruzual & Charlot (2003), we plot the evolution of the Hβ and [MgFe]($=\sqrt{\mathrm{Mg}b \times \mathrm{Fe5015}}$; see Falcón-Barroso 2002) indices with time for a solar metallicity (Fig. 3). The Hβ absorption index is low in very young stars, increases with age until it peaks at around 100–200 Myr, and then decreases with age. Conversely, the [MgFe] index

[1] We have used a modified version of the GANDALF IDL code available at http://www.strw.leidenuniv.nl/sauron/, to include also reddening by dust.

[2] See http://www.ucm.es/info/Astrof/software/indexf/.

remains almost constant for a young population while the Hβ index increases, and increases monotonically with age after the strength of Hβ has peaked.

The values of the Hβ and [MgFe] indices for the nuclear ring hotspots in our sample galaxies are compared to the predicted time-evolution of these indices for SSP models in the left-hand panel of Fig. 3. While some of the data points lie close to the solar metallicity SSP line, most do not, suggesting that a star formation history more complex than an SSP must be responsible for the observed values. On the other hand, the stellar populations in the nuclei of our sample galaxies (Fig. 3, right-hand panel) are well described by SSP models of old ages, and are consistent with previous studies for the nuclear populations of bulges (González Delgado et al. 2004; Sarzi et al. 2005). The star-forming nuclear rings are undoubtedly observed along the same line of sight as an older stellar population in the disc and bulge of their host galaxies. As a consequence, the scenario most likely to match the line strengths of our hotspot spectra is that of a superposition of young stars in the ring, and old stars in the underlying disc and intervening bulge. This situation is similar to the one described in Paper I for NGC 4321, where we used the same indices as shown in Fig. 3.

The larger wavelength range of our present data set allows us to analyse more indices than was possible in Paper I, which enables us to investigate the star formation history of the nuclear rings in more detail. In addition to Hβ and [MgFe], we have measured the HδA (Worthey & Ottaviani 1997) and D(4000) (Bruzual 1983) indices in all the hotspot and nuclear spectra. Like other Balmer indices, the HδA index is an age-sensitive index that is particularly strong in stellar populations with ages 0.1–1 Gyr. The advantage of using higher order Balmer indices such as HδA, however, is that they are much less affected by the presence of emission. The D(4000) index is derived from the ratio of two passbands that lie on either side of the 4000-Å break (see Fig. 2), which occurs as a large number of stellar absorption features appear bluewards of this break in cooler, more opaque stars. In hotter, younger stars, the 4000-Å break is therefore smaller than it is in cooler, older stars.

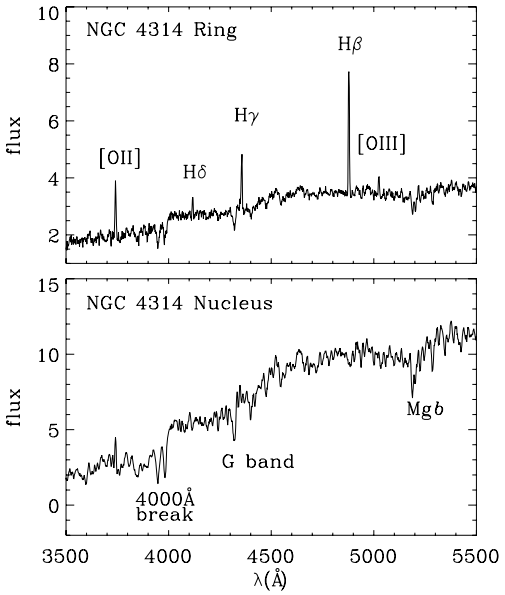

Figure 2. Two examples of the blue spectra obtained, one from the nuclear ring (top panel) and the other from the nucleus (bottom panel) of NGC 4314. The flux scale is in units of 10^{-17} erg cm^{-2} s^{-1} Å^{-1}. Some of the emission and absorption features used in the analysis are identified.

Fig. 4 shows how our HδA and D(4000) measurements compare with the SSP predictions. In the D(4000) versus HδA diagram *none* of the ring hotspot data can be fitted by the SSP model, confirming the need for a combination of young and old stars to explain the spectra of the nuclear ring regions. On the other hand, the nuclear data remain consistent with SSPs. The similarities between the results inferred from the two pairs of absorption-line indices confirm the reliability of the emission-line correction. We note that although SSP models with subsolar metallicities could match the position of some of the hotspot data points in either of the [MgFe] versus Hβ or D(4000) versus HδA diagrams, they could never do so in both diagrams with the same value of the metallicity. Furthermore, no SSP model can match the D(4000) index values below 1.5 observed in many hotspots.

Using the SSP models as a baseline to interpret the index values for the hotspots (as plotted in Figs 3 and 4) as a superposition of young and old stellar populations, we can distinguish two separate groups of objects. The first group includes the majority of the hotspots, for which it would seem plausible to match their position in Figs 3 and 4 by combining $\sim$30−50 Myr young stars with disc and bulge stars older than $\sim$1 Gyr. On the other hand, considerably weaker Hβ and HδA lines in the hotspots of NGC 4314 and NGC 7217 suggest a mixture of even younger ring stars and a disc/bulge population older than $\sim$2.7 Gyr. Assuming that the stellar populations within our nuclear apertures are a good approximation for the underlying disc and bulge populations encompassed by our hotspot spectra, the nuclear data points for NGC 4314 and NGC 7217 further suggest the presence of a much older underlying and intervening stellar population than in the case of our remaining sample galaxies.

In the next section, we will compare the position of the hotspots in the previous diagrams with detailed models featuring a combination of a young ring population with an older disc and bulge stellar population. For simplicity, we will describe the disc and bulge stellar components with a single SSP model. We will allow for more complex star formation histories in the nuclear rings of our sample galaxies than simple instantaneous bursts, considering also a continuous star formation history and multiple starburst episodes.

4.2 Composite stellar population modelling

4.2.1 Instantaneous star formation in the ring

The simplest composite population model for the stellar populations at the hotspot locations assumes that both the young ring population and the older disc and bulge populations can be described by means of SSP models. Fig. 5 shows several of such stellar population models, following the evolution of the line-strength indices ([MgFe] versus Hβ, upper panels; D(4000) versus HδA, lower panels) after the onset of a single instantaneous star formation episode in the ring. From the left-hand to right-hand panels, the models include progressively younger disc and bulge populations, which formed 10, 5 and 3 Gyr before the stars in the ring. In each panel, the strength of the ring starburst is varied, adding from 0.1 to 10 per cent of the mass in the older bulge and disc population.

Starting from the first group of objects, the [MgFe] versus Hβ diagrams of Fig. 5 indicate a rather coherent picture where the majority of the hotspot data points appear to trace the evolution of an SSP $\sim$30−100 Myr after its formation. The figure shows that the bursts contribute $\sim$2 per cent, 2–3 per cent, or 3–5 per cent of the mass of the bulge and disc population, respectively, and indicate slightly older ages for the higher mass fractions. The measurements for NGC 4321 do not suggest such a clean evolution, however, although

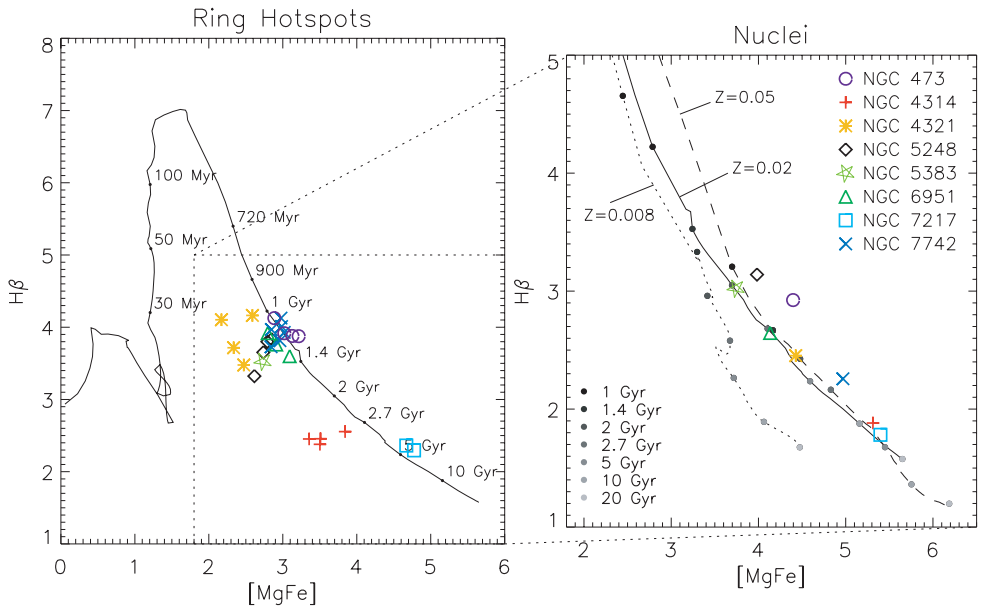

Figure 3. Hβ versus [MgFe] diagram for the ring hotspots and the nuclear regions of our sample galaxies. Left-hand panel: Hβ and [MgFe] line indices for the ring hotspots compared with the predicted time-evolution of the same indices for an single starburst stellar population (SSP) of solar metallicity. Right-hand panel: the same as the left-hand panel but showing the region in the Hβ versus [MgFe] diagram occupied by our nuclear measurements, together with SSP predictions for three different metallicities, as labelled.

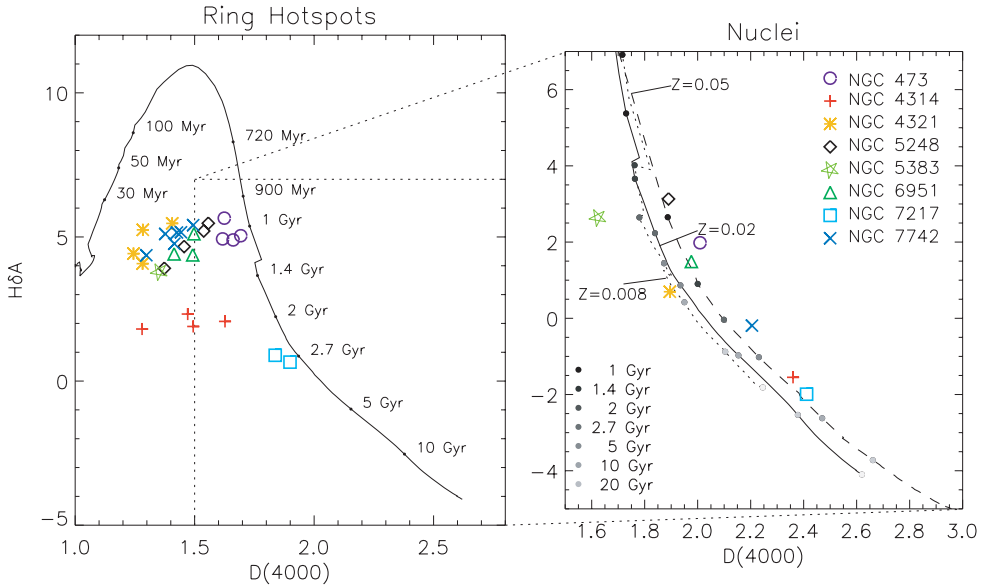

Figure 4. The same as Fig. 3, but now showing the HδA and D(4000) indices. Note the more pronounced discrepancy between the position of the ring hotspots measurements and the predictions of the single starburst model.

they indicate a relatively more massive ring starburst. Excluding this object, the D(4000) versus HδA diagrams yield a rather similar picture for this group of hotspot spectra, in particular when considering the models with a 3-Gyr-old disc and bulge population. In this respect, we note that the template fitting for the hotspot spectra of NGC 4321 was quite poor compared to the rest of the sample, so that the line-strength indices may be somewhat less reliable for this galaxy.

For the hotspots in NGC 4314 and NGC 7217, a bulge and disc population younger than 5 Gyr is ruled out by the [MgFe] versus Hβ diagrams of Fig. 5. For a 10-Gyr-old disc and bulge component, the ring starburst in these galaxies appears to have occurred less than 50 Myr ago and to have contributed less than 1 per cent of the mass. The case for a significantly younger ring population is particularly strong in the case of NGC 4314, since the position of the NGC 7217 data points in the [MgFe] versus Hβ diagram cannot deliver a robust age estimate. Considering that NGC 4314 and NGC 7217 are the galaxies with the earlier Hubble type among our sample, it is possible that the position of their hotspots in Fig. 5 is dictated by a larger intervening bulge population than in the other

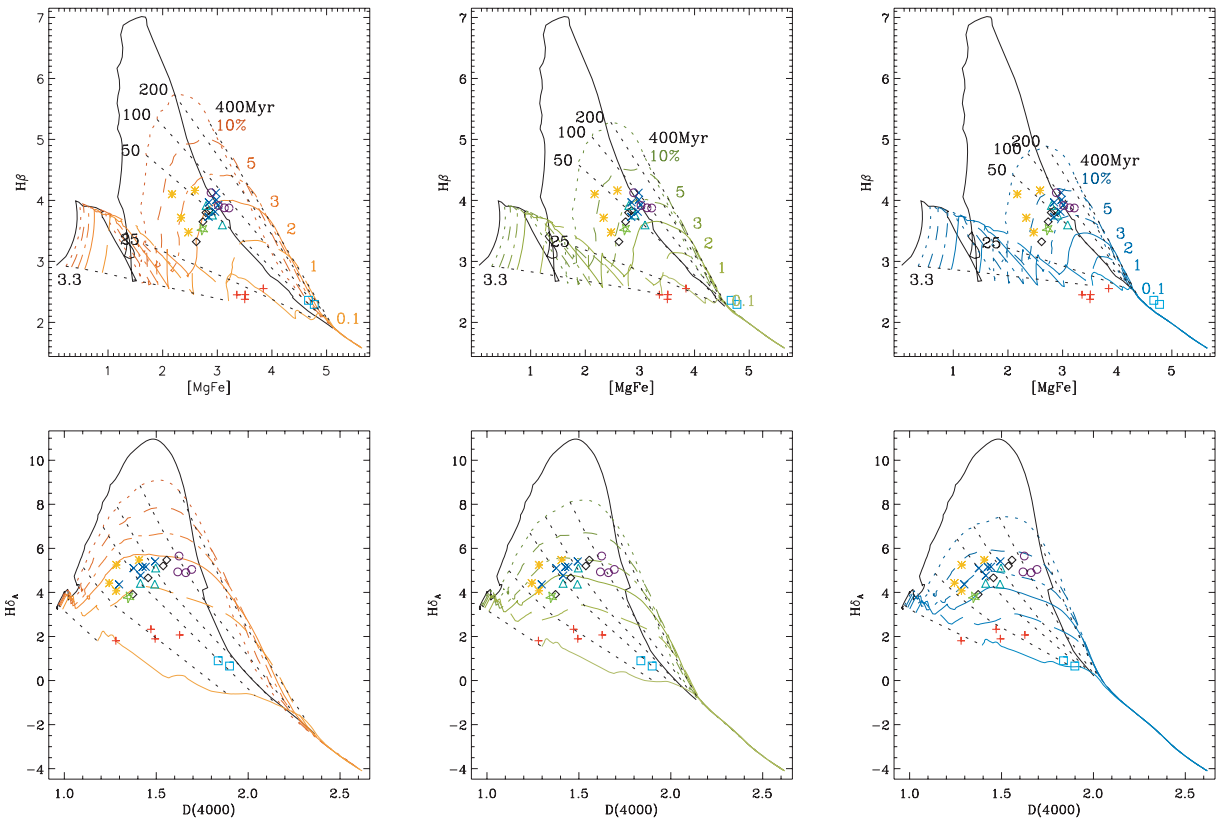

Figure 5. Composite stellar population models for the ring hotspots, assuming the superposition of an old intervening/underlying bulge/disc population and of young ring stars, the latter having formed in a single star formation episode. Both old and young components are assumed to form instantaneously. The upper panels show the evolution of the [MgFe] line-strength index versus that of Hβ, whereas the lower panels show the evolution of D(4000) versus HδA. From the left-hand to right-hand panels, the models include progressively younger disc and bulge populations, which formed 10, 5 and 3 Gyr before the stars in the ring. In all panels, the solid black curve shows, similarly to Figs 3 and 4, the time-evolution of the absorption features in the old bulge and disc population, whereas the coloured curves show the evolution of the same features in the hotspot spectra after the onset of star formation in the ring. In each panel, differently coloured lines show how the strength of the ring starburst is varied, adding from 0.1 to 10 per cent of the mass in the older bulge and disc population, as indentified in the top panels. The positions of the hotspot data points are shown by the coloured symbols, as in Figs 3 and 4.

nuclear rings in our sample, rather than by weaker star formation activity.

Although the properties of an SSP superimposed on an older bulge and disc population can match well the hotspot line indices and provide estimates for the age and mass fraction of the ring populations, in practice such a scenario is quite implausible. The young age of stars in the rings inferred from such models ($\lesssim$30–100 Myr), combined with the relatively high fraction of spiral galaxies with nuclear rings ($\sim$20 per cent, Knapen 2005), would imply that we live in a special time in the history of spiral galaxies. Instead, it is more likely that star formation in nuclear rings has been either continuous in the last few hundred Myr, or characterized by multiple starbursting episodes.

4.2.2 *Continuous star formation in the ring*

To test the first of these classes of models, we compare (Fig. 6) the position of the hotspots in the [MgFe] versus Hβ (upper panels) and D(4000) versus HδA diagrams (lower panels) with the predicted evolution of these indices since the onset of a period of constant star formation activity in the ring. As above, this phase follows the main formation episode for the bulge and disc stars by 10, 5 and 3 Gyr (left-hand, middle and right-hand panels, respectively). As in Fig. 5, the strength of the star formation activity in the ring is a parameter that can be varied: we show models which have added from 0.1 to 10 per cent of the bulge and disc mass after 100 Myr.

There are several inconsistencies between the data and the models in Fig. 6. A continuous star formation scenario underpredicts the strength of the Hδ absorption features in many of the ring hotspot spectra, and cannot account for the values of the Hβ index observed in NGC 7217. Furthermore, the position of different hotspots within the same galaxies, like NGC 7742, NGC 5248 and NGC 4314, suggests that the different regions in the ring are subject to different levels of constant star formation activity that have begun at different epochs, several hundred Myr in the past. This is, however, a most unlikely situation, given that stars and gas circulate along nuclear rings typically in a few tens of Myr.

4.2.3 *Multiple-burst star formation in the ring*

Discarding a history of constant star formation in the rings, we now consider the possibility of multiple starbursting episodes. In Fig. 7, we show the evolution of the line indices for models including from one to five instantaneous bursts, each adding 1 per cent of the bulge and disc mass and occurring every 100 Myr. Because of this periodicity, the model evolution is shown only for the 100 Myr following the last star formation episode. Each of the models includes a disc and bulge population that is 3 Gyr old at the onset of the latest

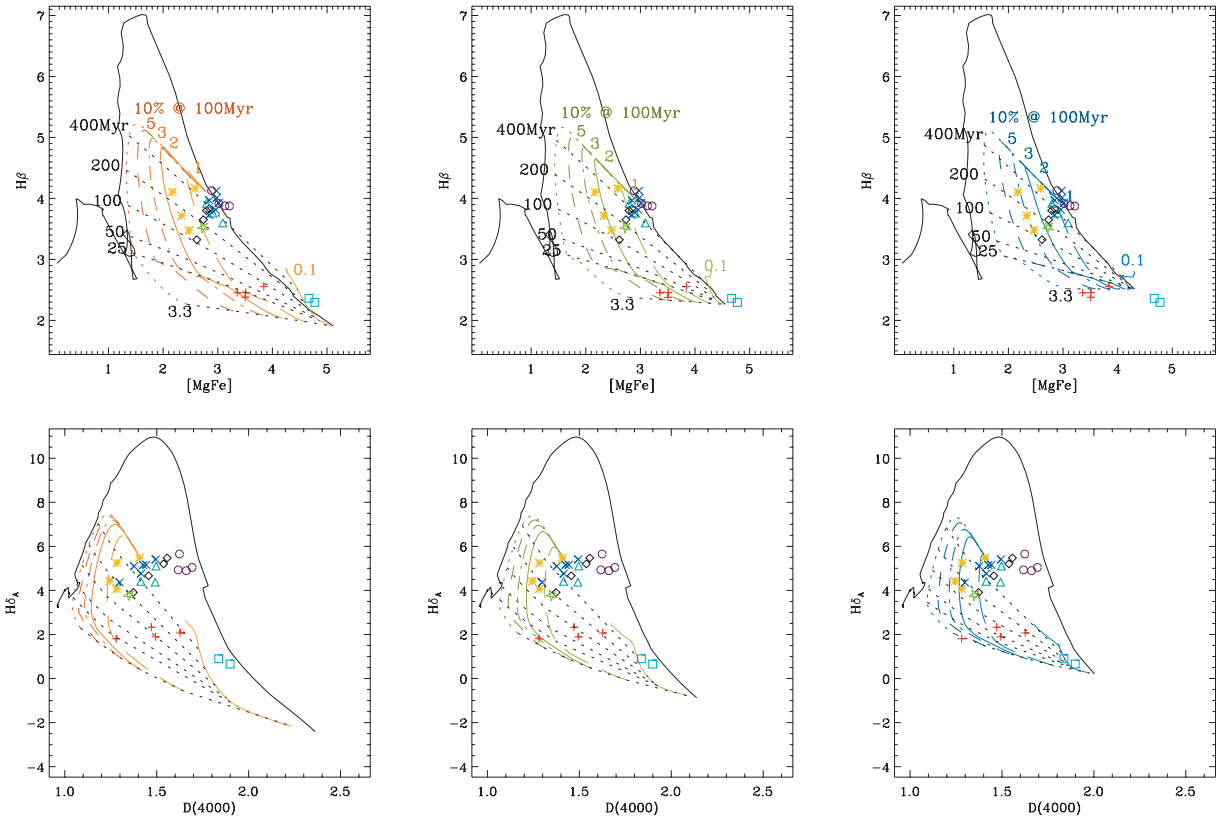

Figure 6. The same as Fig. 5, but now assuming that the ring stars formed over a period of constant star formation. The strength of this activity is quantified by stellar mass that is built in the ring after 100 Myr, relative to the bulge and disc mass.

burst, so that the age of the old stellar component is the same for all models, whereas the recent episodic star formation activity started earlier in models with more such episodes (e.g. star formation in the ring began 400 Myr ago, and 2.6 Gyr after the bulge/disc formation, in a five-burst model). Fig. 7 also shows, for comparison, the composite population models for an instantaneous and continuous star formation scenario in the ring and a 3-Gyr-old disc and bulge population.

Except for NGC 4321 and for the rings requiring very small fractions of young stars (NGC 4314 and NGC 7217), the hotspot data points on both the [MgFe] versus Hβ (upper panels) and D(4000) versus HδA diagrams (lower panels) agree remarkably well with these models for multiple starbursting episodes, suggesting that at least four or three bursts have occurred in the past, as judged from the [MgFe] and D(4000) diagrams, respectively. Similarly to the case of the instantaneous models, we note that the position of the hotspots in NGC 4314 and NGC 7217 in these diagrams can also be matched by models featuring periodic star formation episodes, provided that each burst contributes to mass fractions smaller than 1 per cent and that an older bulge and disc population is included.

4.2.4 Summary of star formation history modelling

Despite the success of the last class of models, the star formation history of nuclear rings is almost certainly more complicated than a simple superposition of instantaneous bursts evenly spaced in time. Some combination of the two latter scenarios is likely, in which star formation events occur episodically, but may vary in length and relative strength. At present, it is impossible to reproduce the *exact* sequence of star formation in the rings from these indices. What is apparent is that the models that most closely match the data points must have a small, but significant, intermediate-age population that is the result of an extended period of recent star formation. They are *not* the result of either continuous star formation, or one single burst of star formation (the present one).

5 EMISSION-LINE DIAGNOSTICS: PHYSICAL CONDITIONS OF THE GAS

In nuclear rings, photoionization by hot OB stars is the most likely source of nebular emission, although shocks may play an additional role. A number of factors determine the appearance of the emission-line spectrum: the metallicity of the gas, the shape of the ionizing radiation spectrum, and the geometric distribution of the gas and ionizing sources (Dopita et al. 2000). The geometry can be combined into one single factor, the mean ionization parameter q (with dimensions cm s^{-1}). This is the ratio of the flux of ionizing photons through a unit area, to the local number density of hydrogen atoms at the edge of the ionized cloud. In this section, we inspect the emission-line spectra of our nuclear rings and nuclei, to determine the gas density, the starburst metallicity, and the ionization parameter. To do this, we will measure the flux ratios of a number of emission lines and compare the observed values to photoionization models.

5.1 Gas density

The two lines in the [S II]$\lambda\lambda$ 6716, 6731 Å doublet have similar excitation levels, but different collisional de-excitation rates. This

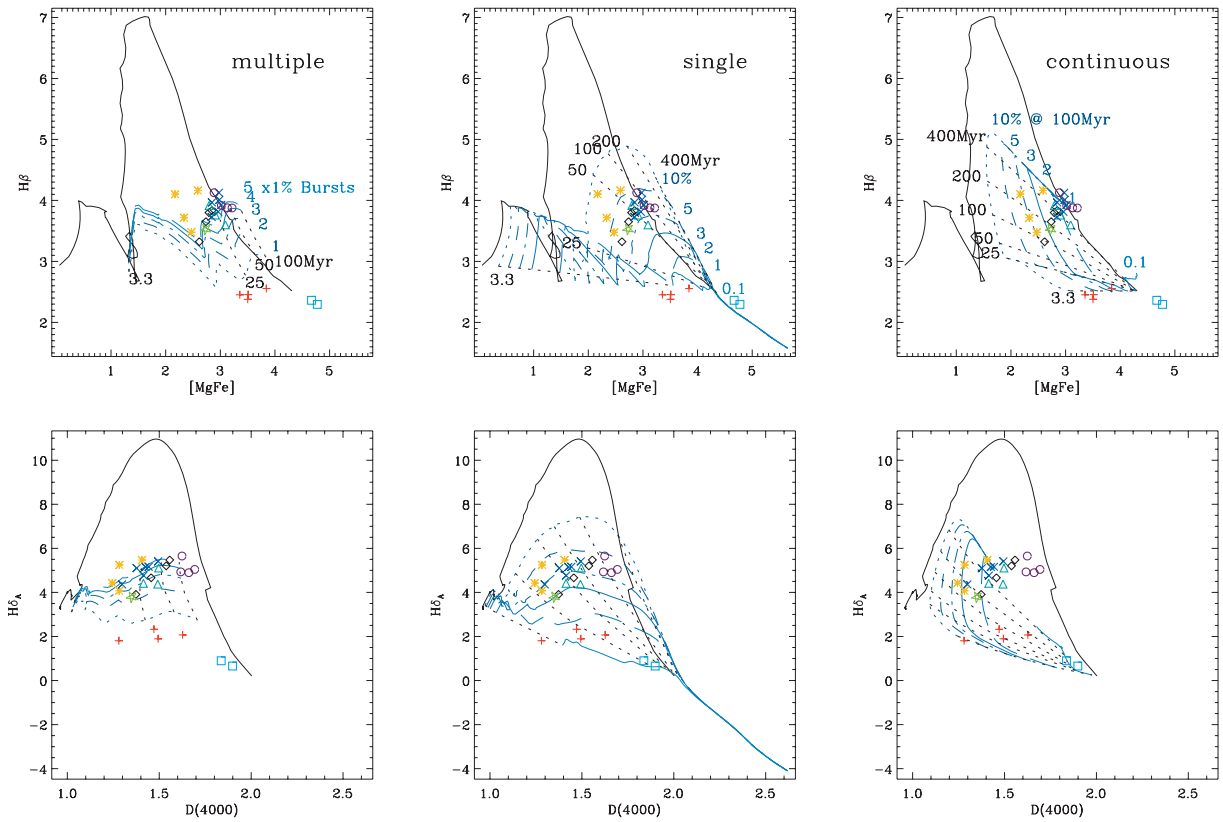

Figure 7. Composite stellar population models for the ring hotspots for the superposition of a 3-Gyr-old bulge/disc population and of young ring stars, which formed during a varying number of instantaneous star formation episodes (from one to five bursts, left-hand panel), during a single burst (middle panel), or over a period of constant star formation (right-hand panel). As in Figs 5 and 6, the top panels show the evolution of [MgFe] versus Hβ, whereas the lower panels show D(4000) versus HδA. The middle and right-hand panels are similar to the right-hand panels of Figs 5 and 6, respectively. The multiburst model (left-hand panel) shows the time-evolution of the indices in the hotspot spectra since the onset of the last starburst, each of which is set to contribute 1 per cent of the bulge and disc mass.

results in the relative populations of the two levels being mostly dependent on the gas electron density (Seaton 1954), which can therefore be estimated from the intensity ratio of these lines. Fig. 8 shows the [S II]λ6716/[S II]λ6731 ratio for the nuclear rings in our sample. The electron densities, indicated by the dashed lines, are for a typical temperature of $T = 10^4$ K (Osterbrock 1989). The nuclear rings show a wide range in electron density, both within each ring, and across the sample. Most of the rings fall within the range $N_e = 10-350\,\mathrm{cm}^{-3}$, with NGC 6951 and NGC 7217 having higher densities, of up to $800\,\mathrm{cm}^{-3}$. This is consistent with previous studies: Kennicutt, Keel & Blaha (1989) found a wide range of electron densities, from $N_e = 10-1000\,\mathrm{cm}^{-3}$, for a number of H II regions, which included both disc and circumnuclear H II regions. Similar results were found by Ho, Filippenko & Sargent (1997).

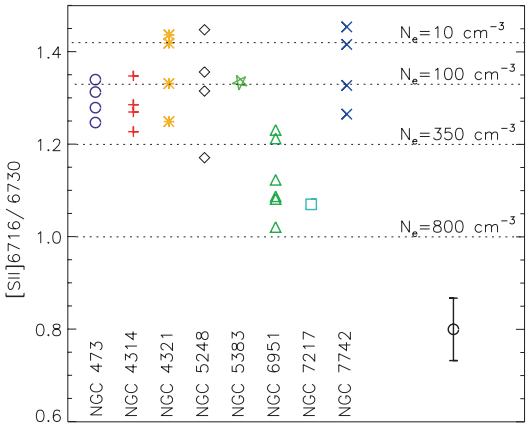

Figure 8. The [S II]λ6716/[S II]λ6731 ratio in the nuclear rings of our sample galaxies. Assuming a temperature of 10^4 K, the dashed lines give estimates of the electron density. For NGC 7217, the two hotspot spectra were combined to achieve a minimum S/N of 3 for the [S II]λ6716/[S II]λ6731 ratio. The error bar shown at the bottom right-hand side of the plot is the average uncertainty measured within our sample.

5.2 Metallicity and ionization parameter

Veilleux & Osterbrock (1987; hereafter V087) devised a classification system based on the ratios of forbidden to hydrogen lines in order to separate gas emission originating in H II regions from nebular activity powered by other sources of ionization such as active galactic nuclei (AGN). Their ratios involve lines which are close together in wavelength, minimizing errors in calibration and reddening correction, such as the [O III]λ5007/Hβ ratio in blue spectra, and the [N II]λ6583/Hα, [S II]$\lambda\lambda$6716,6731/Hα and [O I]λ6300/Hα in red spectra. When the [O III]/Hβ ratio is plotted against any of the red line ratios, different types of emission-line galaxies occupy different regions of the diagrams. H II regions and H II nuclei in particular tend to be located in narrow, well-defined zones (Kewley

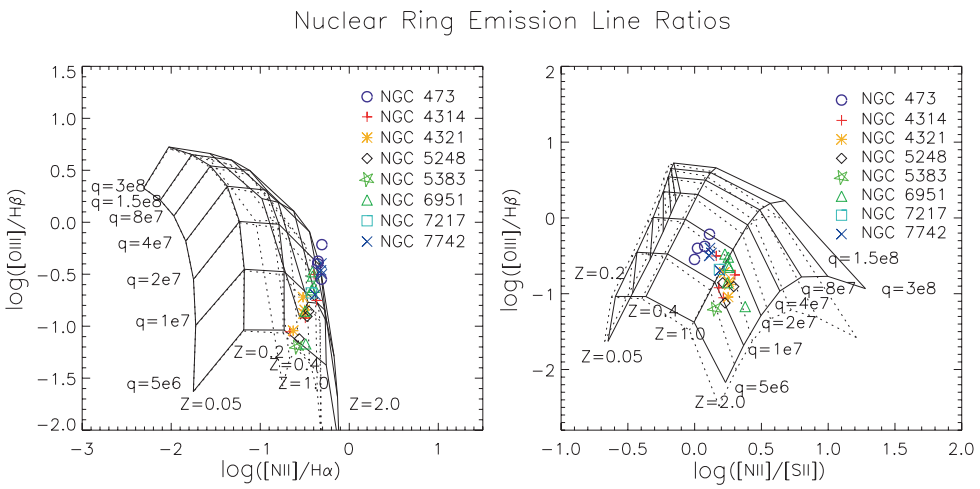

Figure 9. Diagnostic diagrams of log([O III]/Hβ) versus log([[N II]/Hα) (left-hand panel) and log([O III]/Hβ) versus log([N II]/[S II]) (right-hand panel), featuring the MAPPINGS III model prediction for the nebular emission arising in star-forming regions. The models are based on STARBURST99 spectral energy distributions for continuous star formation over a period of 8 Myr. The theoretical grids assume different values for the ionization parameter and for the starburst metallicity, and are shown with the black lines for a density of 10 cm^{-3} and the dashed lines for a density of 350 cm^{-3}. The data points measured from the nuclear ring hotspots are shown as the coloured symbols. Uncertainties in the ratios are at most 30 per cent, translating into error bars of 0.1 or less along both the axes of these logarithmic plots.

et al. 2001) in such diagnostic diagrams, which can be understood by means of sophisticated photoionization models.

In this respect, Dopita et al. (2000) and Kewley et al. (2001) present valuable models for H II regions obtained with the photoionization code MAPPINGS III (Sutherland & Dopita 1993) while using the PEGASE (Fioc & Rocca-Volmerange 1997) and STARBURST99 (Leitherer et al. 1999) codes to generate the stellar ionizing radiation fields that depend on the metallicity of the starburst. Fig. 9 shows an example of a photoionization grid, calculated in the case of the [O III]/Hβ versus [N II]/Hα diagnostic diagram for metallicities 0.05, 0.2, 0.4, 1 and 2 times solar, values of the ionization parameter $q = 3 \times 10^8, 1.5 \times 10^8, 8 \times 10^7, 4 \times 10^7, 2 \times 10^7, 1 \times 10^7$ and 5×10^6 cm s^{-1}, and for densities of $N_e = 10$ and 350 cm^{-3}. The narrow zone occupied by H II regions and H II nuclei in this plot coincides with the folding of the ionization parameter/metallicity surface: H II regions characterized by a large range in metallicity or ionization parameter are projected into a narrow band on the figure. Theses starburst models set tight upper limits for the values of these line ratios, so that emission-line regions that lie above and to the right-hand side of the model grids must have other source of ionization beside, or in addition to, O stars (Kewley et al. 2001).

Although star-forming regions are readily identified in VO87 diagrams such as the one juxtaposing [OIII]/Hβ with [N II]/Hα, the folded nature of the models makes it difficult to determine unambiguously the metallicity and the ionization parameter of star-forming regions, except for very low metallicities. Dopita et al. (2000) and Kewley et al. (2001) found that the best combination of line ratios for separating metallicity and ionization parameter effects are [N II]$\lambda\lambda$6548,6583/[O II]$\lambda\lambda$3727,3729 versus [O III]λ5007/[O II]$\lambda\lambda$3727,3729, or [N II]/[O II] versus [O III]/Hβ. Although all these lines fall within the wavelength range of our spectra, we cannot measure the [N II]/[O II] ratio with confidence, since we do not dispose of an accurate relative flux-calibration of our red and blue spectra, where the [N II] and [O II] lines are found, respectively. Additionally, the [O II] lines are not always observed. To estimate the metallicity and ionizing parameter of the emission-line regions observed by our spectra, we can instead use the diagnostic diagram based on the [N II]λ6583/[S II] and [O III]/Hβ ratios. Rubin, Ford & Whitmore (1984) were the first to suggest the [N II]/[S II] ratio as a metallicity indicator, and Kewley & Dopita (2002) recently confirmed the usefulness of this ratio for estimating metallicities from slightly subsolar to supersolar values, making [N II]/[S II] quite complementary to [N II]/Hα in this respect. This is illustrated by the MAPPINGS III models plotted in the right-hand panel of Fig. 9, where the model grid in the [N II]/[S II] diagram folds only at very low metallicity.

Fig. 9 shows the [O III]/Hβ, [N II]/Hα and [N II]/[S II] line ratios measured in the ring hotspots. The location of the ring data in the [N II]/Hα diagram is consistent with nebular emission powered only by O stars, although no conclusion on the metallicity of the starburst can be drawn from this VO87 diagram. On the other hand, the position of the data points in the [N II]/[S II] versus [O III]/Hβ grid indicates that the ring hotspots are populated by H II regions with metallicities ranging from slightly below to just above solar, with values for the ionization parameter between 1 and 2×10^7 cm s^{-1}.

Two aspects of this emission-line analysis are also relevant to the our stellar population results. First, Fig. 9 firmly rejects starbursts of exceedingly low metallicity, thus further excluding the possibility discussed in Section 4.1 that the position of some of the line-strength measurements in the ring hotspots could be consistent with SSP models with subsolar metallicity. Secondly, the model grids of Fig. 9 use a spectral energy distribution that was obtained from STARBURST99 and assuming continuous star formation over a short period of 8 Myr. Models based on a truly instantaneous star formation event were found to be grossly inconsistent with the data, producing exceedingly high [O III]/Hβ ratio compared to the values measured in the ring hotspots. This further supports the statement made in Section 4.2, that the star formation history of nuclear rings is likely to be a combination of continuous and episodic bursts.

5.3 Line ratios for the nuclei

All the observed nuclei in the sample have measurable emission lines. Some of the galaxies are classified as AGN in the literature,

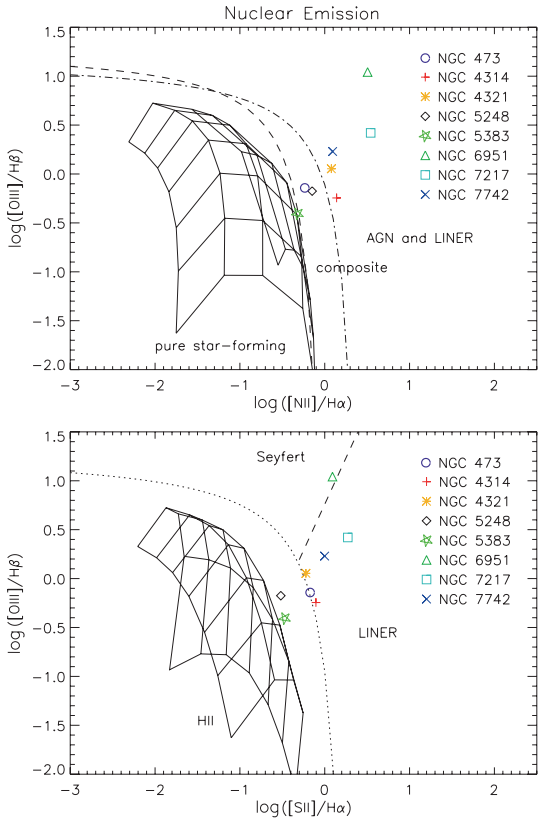

Figure 10. Diagnostic diagrams of log([O III]/Hβ) versus log([N II]/Hα) (upper panel) and versus log([S II]/Hα) (lower panel), compared with theoretical model grids as in Fig. 9. The data points measured from the nucleus of each galaxy are plotted as the coloured symbols. Upper panel: the dot–dashed line is the 'maximum starburst line' of Kewley et al. (2001). The dashed line is the empirically derived starburst line from Kauffmann et al. (2003). Lower panel: the dotted line is the 'maximum starburst line' of Kewley et al. (2001), and the dashed line from Kewley et al. (2006), to separate Seyferts and LINERs.

others as H II nuclei or Low-Ionization Nuclear Emission Regions (LINERs, Heckman 1980). Baldwin, Phillips & Terlevich (1981) and, later, VO87 reported that the [O III]/Hβ versus [N II]/Hα diagram allows one to distinguish between the different types of nuclei. This work has been extended by Kewley et al. (2001), who determined a theoretical 'maximum starburst line': galaxies above this line are likely to be dominated by an AGN. Kauffmann et al. (2003) modified this scheme to include an empirically derived line dividing pure star-forming galaxies from Seyfert–H II composite objects. These classification lines can be seen in the top panel of Fig. 10, compared to the ratios derived for the nuclear regions of the galaxies in the present sample. NGC 5383 is closest to possessing a purely star-forming nucleus, NGC 473 and NGC 5248 are classified as composite, and the rest fall in the LINER and AGN category.

Kewley et al. (2006) have extended the scheme even further, using the [O III]/Hβ versus [S II]/Hα plot to separate AGN from LINER activity. This can be seen for our data in the lower panel of Fig. 10. In this diagram, NGC 6951 is the only Seyfert nucleus, NGC 7217 and NGC 7742 are well within the region occupied by LINERs, NGC5383 and NGC5248 remain close to the H II-region model grids, and each of the remaining nuclei lies on the line between LINER and star-forming activity, suggesting a composite nature. These results are in remarkable agreement with the Palomar classification for these nuclei (Table 1), with the possible exception of NGC4314, for which our data suggest a composite classification rather than a strict LINER activity. NGC 473 was not observed by Ho et al., and our data suggest a H2/T2 nuclear classification.

6 DISCUSSION

6.1 The star formation history of nuclear rings

In Paper I, we have investigated the star formation history in the nuclear ring of NGC 4321 using the three line-strength indices that can be probed by the SAURON integral-field spectrograph, namely Hβ, Fe5015 and Mg*b*. For NGC 4321 we concluded that star formation in the ring was likely long lived and episodic, thus arguing that the nuclear ring is a stable configuration that is intimately linked to the large bar in this galaxy (Knapen et al. 1995b).

In this paper, we have measured the strength of two additional stellar features, the 4000-Å break and the Hδ absorption line, in the nuclear rings of eight nearby galaxies. By comparing the observed values for all five indices to the predictions of population synthesis models for the star formation history in the ring, we have reached a similar conclusion to Paper I – that star formation in nuclear rings is a prolonged and episodic phenomenon.

Models, assuming that nuclear rings form single instantaneous burst of star formation, yield predictions that are not incompatible with the data, but such a scenario is generally ruled out because it implies formation epochs for the rings that are too short and recent to be consistent with the relatively high frequency of occurrence of nuclear rings in nearby galaxies (Section 4.2.1). Furthermore, the inclusion of the *D*(4000) and HδA indices in our analysis allowed us to firmly rule out the possibility of a history of continuous star formation for our nuclear rings (Section 4.2.2). On the other hand, the strength of the absorption lines in the ring hotspot spectra is well matched by models allowing for the formation of the ring stars over a number of instantaneous star formation episodes, superimposed on an underlying or intervening old disc and bulge population (Section 4.2.3).

The success of this family of models, together with the demise of its alternatives, confirm the general understanding that after the initial formation of the bulge and disc component, gaseous material is transported towards the centre over a prolonged period of time, where it accumulates near the location of the ILR and where the density threshold for the ignition of star formation is repeatedly crossed. The inflow of gaseous material can be driven by the presence of large-scale bars, but this is not the only mechanism that can fuel the circumnuclear region (see e.g. Knapen et al. 2004 for a case study of ring formation induced by a minor merger). In fact, two of our sample galaxies are classified as unbarred and they will be further discussed below. Another object that will deserve further attention is NGC 4314, for which our modelling suggests that the ring stars have formed very recently, only a few Myr ago. Below, we will discuss the possibility that for NGC 4314 we could be witnessing the initial phases of ring formation.

Our results on the star formation history of nuclear rings have several important consequences. As previously stated, nuclear rings are common in spiral galaxies, and are characterized by high star formation rates. If nuclear rings form stars over a long time-scale, this will lead to the the accumulation of considerable stellar masses in the central regions of their host galaxies. Kormendy & Kennicutt (2004) estimated that for the typical mass of molecular gas and star formation rate of nuclear rings, stellar masses of 10^8–10^9 M$_\odot$ will be formed. In Paper I, the nuclear ring in NGC 4321 was observed

to be thicker when viewed in stellar indices than when viewed in Hβ emission, indicating that the new stars are diffusing out of the ring. It is possible that these stars will diffuse further in the galactic disc, contributing to the formation of a more bulge-like structure due to vertical instabilities triggered by the presence of a bar. First characterized as pseudo-bulges by Kormendy (1993), such structures half-way between bulges and discs may be an integral component of most spiral galaxies, in particular in those of later Hubble types. Kormendy & Kennicutt (2004) further discuss how pseudo-bulges are a consequence of slow secular processes, pointing out how secular evolution becomes more important than galaxy mergers or interactions in re-shaping the structure of galaxies as the Universe expands.

If nuclear rings are stable configurations in disc galaxies that add considerable stellar mass to the centres of their hosts over prolonged periods of star formation, nuclear rings should be regarded as a key component in the secular evolution of galaxies. Furthermore, nuclear rings may be even more frequent than previously thought. Most nuclear rings, and all those used by Knapen (2005) to derive the fraction of nuclear ring in local spirals, were identified using Hα imaging that traces massive star formation. Yet, our stellar population modelling suggests that over most of their lifetime nuclear rings are not actively forming massive stars, which implies that a significant but so-far-unknown fraction of galaxies could host a young nuclear ring that is presently not forming massive stars. The confirmation of nuclear rings as an established feature of a galaxy also reinforces the view that nuclear rings are linked to the large-scale bar, and the connection between nuclear rings and ILRs.

6.2 NGC 4314

Our stellar absorption-line measurements show how NGC 4314 stands apart from the majority of the rings in our sample, with a significantly older underlying or intervening disc and bulge population and much younger ring stars. This conclusion is consistent with the findings of Benedict et al. (2002), who analysed high spatial resolution optical colour maps obtained with the *Hubble Space Telescope* (*HST*) to study the ages of the single star clusters in the ring. They found colours consistent with instantaneous star formation and little evidence for any cluster older than 40 Myr in the ring. Although the analysis of Benedict et al. did not cover the intracluster stellar population, which also contribute to our hotspot spectra, the absence of clusters older than 40 Myr suggests that no star formation episode occurred in the ring of NGC 4314 previous to the present one.

It would thus appear that in the case of NGC 4314 we are witnessing the initial massive star formation event, which may well coincide with the formation of the nuclear ring. The observed blue stellar arms just outside the nuclear ring (Benedict et al. 2002) are evidence for star formation activity in the recent past (between 100 and 200 Myr ago) but whether this occurred within the present configuration of the ring, or within a larger past version of it (as suggested by Combes et al. 1992), is not presently clear. What is evident is that NGC 4314 is peculiar among our sample galaxies also because the massive star formation in the entire galaxy is practically confined to the nuclear ring (known since Burbidge & Burbidge 1962), and because the galaxy is particularly deficient of atomic hydrogen gas, H I (García-Barreto et al. 1991; Combes et al. 1992). These pecularities make the conclusion that we are indeed witnessing the very first phase of massive star formation in the nuclear ring less unattractive than it might seem at first glance when compared to the results for the other rings in our sample.

6.3 Unbarred galaxies: NGC 7217 and NGC 7742

NGC 7217 and NGC 7742 are both classified as unbarred galaxies and indeed appear very symmetric in near-IR 2MASS images. Using ground-based and *HST* near-IR imaging, Laine et al. (2002) confirm that no bars can be found in NGC 7217, but find two small bars in NGC 7742 (with deprojected bar radii of 1.2 and 6.8 arcsec, corresponding to 130 and 730 pc). The lack of a large bar in both cases may initially seem problematic, as the general picture of nuclear ring formation is often described as requiring a bar to drive gas towards the centre. There are other ways of achieving a non-axisymmetric potential which can stimulate inflow, however, such as the presence of an oval distortion, or the influence of external forces. Both NGC 7217 and NGC 7742 have counter-rotating subsystems (Merrifield & Kuijken 1994; Sil'chenko & Afanasiev 2000; de Zeeuw et al. 2002), which hints at a turbulent, merger, history.

NGC 7742 has a counter-rotating gas system, and NGC 7217 has a counter-rotating stellar system. Sil'chenko & Moiseev (2006) suggest that the two galaxies have undergone a similar past interaction. They propose that NGC 7742 has only recently started accreting gas, while NGC 7217 is at a later stage of evolution and has already converted its counter-rotating gas into stars. Mazzuca et al. (2006) find that the metallicity of the gas in the ring of NGC 7742 is close to solar, in agreement with our results. As there are no suitable large metal-rich companion galaxies with which NGC 7742 can have interacted, Mazzuca et al. propose that a smaller, metal-poor dwarf galaxy has been cannibalized. Part of its gas was then concentrated in the ring, where star formation proceeded long enough for the metallicity to reach a solar value. They estimate that this process takes a few tens of Myr, which agrees with our stellar population modelling for this galaxy.

Buta et al. (1995) and Combes et al. (2004) suggest that the oval distortion present in NGC 7217 would be sufficient to create the resonances which shape the three rings which it possesses, without invoking a minor merger explanation, and the detection of a counter-rotating stellar system could be attributed to a large bulge velocity dispersion. They also highlight that a number of nuclear rings are present in NGC 7217, all found at different radii. The smallest is a red dust ring, followed radially outwards by an Hα ring, which in turn is followed by a broad red ring. Like NGC 4314, NGC 7217 is also deficient in H I gas (Buta et al. 1995), and both have much older underlying stellar populations (Fig. 3) than the other galaxies in our sample.

6.4 Absence of Wolf–Rayet features

Wolf–Rayet (WR) stars are the remnants of the most-massive stars in galaxies. Their numbers therefore peak shortly after a major star formation episode, typically when the starburst is only 3–4 Myr old. The number and type of WR stars is also a strong function of the starburst metallicity, a fact that stimulated the study of WR stars as a means to trace the nature of massive star formation in external galaxies (e.g. Vacca & Conti 1992; Shaerer & Vacca 1998; Shaerer, Contini & Kunth 1999; Guseva, Izotov & Thuan 2000). In optical spectra, the most notable WR feature is the so-called 4650-Å 'bump', which is due to a superposition of broad stellar emission lines.

In *none* of our ring hotspot spectra is such a feature observed. The absence of WR features suggests that the *bulk* of the young stars in the ring regions subtended by our spectra have formed over a longer period of time than just a few Myr, consistent with our absorption-line analysis. The only exception to this statement is

NGC 4314. For this galaxy we have evidence that the hotspot spectra are a superposition of an old bulge and disc stellar population with very young ring stars, less than 25 Myr old. A 4650-Å 'bump' could therefore be expected in this case, and that this feature is not observed could be due to a strong contamination of intervening bulge stars, consistent with the early-type classification of this disc galaxy (see also Section 4.2.1)

7 CONCLUSIONS

We present a study of the optical spectra of a sample of eight star-forming nuclear rings and the nuclei of their host galaxies. These spectra cover a wide range in wavelength, and allow us to measure a number of gaseous and stellar features. The stellar absorption indices show that along the line of sight to the nuclear ring we can detect the older underlying and intervening disc and bulge, as well as the young stars being formed in the ring. We use two absorption-line index diagrams, Hβ versus MgFe and HδA versus D(4000), to test models for the star formation history of the rings. The simultaneous use of these indices allows us to rule out a constant star formation history, whereas the possibility that these rings' one-off events in a galaxy's history are discarded on the basis that it would be unlikely to observe all these rings shortly after they have formed. Our models suggest instead that nuclear rings are in fact more long-lived structures with extended, although episodic, periods of star formation. The absence of WR features in our spectra further shows that nuclear rings are not made exclusively of stars that formed only very recently. These results confirm not only the intimate dynamical connection between nuclear rings and their host galaxies, but also the important role that the rings can play in transforming disc gas to (pseudo-)bulge stars, thus stimulating secular evolution.

The gas emission lines of the nuclear rings reveal that the rings possess a range of electron densities, most within a range of 10–350 cm^{-3}. Diagnostic diagrams show that all rings are populated by H II regions with similar ionization parameters and with a small spread in metallicity around the solar value.

The nuclear rings of NGC 4314 and NGC 7217 stand apart from the other nuclear rings in the sample, as they appear to have much older and prominent underlying populations. They also have much lower values of the Hβ and HδA indices, which in the case of NGC 4314 implies much younger ages for the ring stars. In this galaxy, which stands out from the rest of the sample for its lack of star formation in the disc and its deficiency of neutral gas, we may be witnessing the initial phases of the ring formation. The vast majority of the nuclear rings in the sample can thus be described by a scenario where the nuclear ring is a stable structure, in most cases induced by the bar, and confirming that all these rings have formed by dynamical means near the ILRs. This is also true for the two galaxies in our sample which lack a prominent large bar, but for which a past minor merger event may well have caused a similar non-axisymmetry in the galaxy's gravitational potential.

Our study of the spectra of the nuclei of our sample galaxies shows that all display emission lines. Consistent with previous studies for the nuclear activity and stellar populations, the majority of our nuclei appear to be dominated by old stellar populations and by LINER-like emission.

ACKNOWLEDGMENTS

We thank the referee, Hervé Wozniak, for his useful comments. This work is based on observations made with the WHT, operated on the island of La Palma by the Isaac Newton Group in the Spanish Observatorio del Roque de los Muchachos of the Instituto de Astrofísica de Canarias. ELA was supported by a PPARC studentship. JHK acknowledges the Leverhulme Trust for the award of a Leverhulme Research Fellowship.

REFERENCES

Allard E. L., Peletier R. F., Knapen J. H., 2005, ApJ, 633, L25
Allard E. L., Knapen J. H., Peletier R. F., Sarzi M., 2006, MNRAS, 371, 1087 (Paper I)
Alonso-Herrero A., Ryder S. D., Knapen J. H., 2001, MNRAS, 322, 757
Arsenault R., Boulesteix J., Georgelin Y., Roy J. R., 1988, A&A, 200, 29
Athanassoula E., 1992, MNRAS, 259, 345
Baldwin J. A., Phillips M. M., Terlevich R., 1981, PASP, 93, 5
Barth A. J., Ho L. C., Filippenko A. V., Sargent W. L. W., 1995, AJ, 110, 1009
Benedict G. F., Higdon J. L., Tollestrup E. V., Hahn J. M., Harvey P. M., 1992, AJ, 103, 757
Benedict G. F., Smith B. J., Kenney J. D. P., 1996, AJ, 111, 1861
Benedict G. F., Howell D. A., Jørgensen I., Kenney J. D. P., Smith B. J., 2002, AJ, 123, 1411
Bruzual A. G., 1983, ApJ, 273, 105
Bruzual G., Charlot S., 2003, MNRAS, 344, 1000
Burbidge E. M., Burbidge G. R., 1962, ApJ, 135, 694
Buta R., Crocker D. A., 1991, AJ, 102, 1715
Buta R., van Driel W., Braine J., Combes F., Wakamatsu K., Sofue Y.,Tomita A., 1995, ApJ, 450, 593
Combes F., 1988, in Dickman R. L., Snell R. L., Young J. S., eds, Molecular Clouds in the Milky Way and External Galaxies. Springer-Verlag, Berlin, p. 441
Combes F., Gerin M., 1985, A&A, 150, 327
Combes F., Gerin M., Nakai N., Kawabe R., Shaw M. A., 1992, A&A, 259, L27
Combes F. et al., 2004, A&A, 414, 857
de Vaucouleurs G., 1963, ApJS, 8, 31
de Zeeuw P. T. et al., 2002, MNRAS, 329, 513
Díaz-Santos T., Alonso-Herrero A., Colina L., Ryder S. D., Knapen J. H., 2007, ApJ, 661, 149
Dopita M. A., Kewley L. J., Heisler C. A., Sutherland R. S., 2000, ApJ, 542, 224
Elmegreen B. G., 1999, in Beckman J. E., Mahoney T. J., eds, ASP Conf. Ser. Vol. 187, The Evolution of Galaxies on Cosmological Timescales. Astron. Soc. Pac., San Francisco, p. 145
Elmegreen B. G. et al., 1998, ApJ, 503, L119
Elmegreen B. G., Elmegreen D. M., Hirst A. C., 2004, ApJ, 612, 191
Engelbracht C. W., Rieke M. J., Rieke G. H., Kelly D. M.,Achtermann J. M., 1998, ApJ, 505, 639
Erwin P., Sparke L. S., 2002, AJ, 124, 65
Erwin P., Vega Beltran J. C., Beckman J. E., 2001, in Knapen J. H., Beckman J. E., Shlosman I., Mahoney T. J., eds, ASP Conf. Ser. Vol. 249, The Central Kiloparsec of Starbursts and AGN: The La Palma Connection. Astron. Soc. Pac., San Francisco, p. 171
Eskridge P. B. et al., 2000, AJ, 119, 536
Falcón-Barroso J., 2002, PhD thesis, Univ. Nottingham
Fathi K., van de Ven G., Peletier R. F., Emsellem E., Falcón-Barroso J., Cappellari M., de Zeeuw T., 2005, MNRAS, 364, 773
Fioc M., Rocca-Volmerange B., 1997, A&A, 326, 950
García-Barreto J. A., Downes D., Combes F., Gerin M., Magri C., Carrasco L., Cruz-Gonzalez I., 1991, A&A, 244, 257
Grosbøl P., Patsis P. A., Pompei E., 2004, A&A, 423, 849
González Delgado R. M., Cid Fernandes R., Pérez E., Martins L. P., Storchi-Bergmann T., Schmitt H., Heckman T., Leitherer C., 2004, ApJ, 605, 127
Guseva N. G., Izotov Y. I., Thuan T. X., 2000, ApJ, 531, 776
Harris J., Calzetti D., Gallagher J. S. III, Conselice C. J., Smith D. A., 2001, AJ, 122, 3046

Heckman T. M., 1980, A&A, 88, 365
Heller C., Shlosman I., 1994, ApJ, 424, 84
Ho L. C., Filippenko A. V., Sargent W. L. W., 1997, ApJS, 112, 315
Huntley J. M., Sanders R. H., Roberts W. W., 1978, ApJ, 221, 521
Jogee S., Shlosman I., Laine S., Englmaier P., Knapen J. H., Scoville N. Z., Wilson C. D., 2002, ApJ, 575, 156
Jogee S. et al., 2004, ApJ, 615, L105
Kauffmann G. et al., 2003, MNRAS, 346, 1055
Kennicutt R. C., Keel W. C., Blaha C. A., 1989, AJ, 97, 1022
Kewley L. J., Dopita M. A., 2002, ApJS, 142, 35
Kewley L. J., Dopita M. A., Sutherland R. S., Heisler C. A., Trevena J., 2001, ApJ, 556, 121
Kewley L. J., Groves B., Kauffmann G., Heckman T., 2006, MNRAS, 372, 961
Kotilainen J. K., Reunanen J., Laine S., Ryder S. D., 2000, A&A, 353, 834
Knapen J. H., 2005, A&A, 429, 141
Knapen J. H., Beckman J. E., Shlosman I., Peletier R. F., Heller C. H., de Jong R. S., 1995a, ApJ, 443, L73
Knapen J. H., Beckman J. E., Heller C. H., Shlosman I., de Jong R. S., 1995b, ApJ, 454, 623
Knapen J. H., Shlosman I., Peletier R. F., 2000, ApJ, 529, 93
Knapen J. H., Whyte L. F., de Blok W. J. G., van der Hulst J. M., 2004, A&A, 423, 481
Knapen J. H., Mazzuca L. M., Böker T., Shlosman I., Colina L., Combes F., Axon D. J., 2006, A&A, 448, 489
Kormendy J., 1993, in DeJonghe H.,Habing H. J., eds, IAU Symp., 153, Galactic Bulges. Dordrecht, Kluwer, p. 209
Kormendy J., Kennicutt R. C., 2004, ARA&A, 42, 603
Kuntschner H. et al., 2006, MNRAS, 369, 497
Laine S., Shlosman I., Knapen J. H., Peletier R. F., 2002, ApJ, 567, 97
Leitherer C. et al., 1999, ApJS, 123, 3
Maraston C., 2005, MNRAS, 362, 799
Mazzuca L. M., Sarzi M., Knapen J. H., Veilleux S., Swaters R., 2006, ApJ, 649, L77
Mazzuca L. M., Knapen J. H., Veilleux S., Regan M. W., 2007, ApJ, submitted
Merrifield M. R., Kuijken K., 1994, ApJ, 432, 575
Osterbrock D. E., 1989, Astrophysics of Gaseous Nebulae and Active Galactic Nuclei. Univ. Science Books, Mill Valley
Pogge R. W., 1989, ApJS, 71, 433
Puxley P. J., Brand P. W. J. L., 1999, ApJ, 514, 675
Ryder S. D., Knapen J. H., 1999, MNRAS, 302, L7
Ryder S. D., Knapen J. H., Takamiya M., 2001, MNRAS, 323, 663
Rubin V. C., Ford W. K. Jr, Whitmore B. C., 1984, ApJ, 281, 21
Sanders R. H., Tubbs A. D., 1980, ApJ, 235, 803
Sarzi M., Rix H. W., Shields J. C., Ho L. C., Barth A. J., Rudnick. G., Filippenko A. V., Sargent W. L. W., 2005, ApJ, 628, 169
Sarzi M. et al., 2006, MNRAS, 366, 1151
Schwarz M. P., 1984, MNRAS, 209, 93
Seaton M. J., 1954, MNRAS, 114, 154
Sellwood J. A., Wilkinson A., 1993, Rep. Prog. Phys., 56, 173
Sil'chenko O. K., Afanasiev V. L., 2000, A&A, 364, 479
Sil'chenko O. K., Moiseev A. V., 2006, AJ, 131, 1336
Simkin S. M., Su H. J., Schwarz M. P., 1980, ApJ, 237, 404
Shields J. C. et al., 2007, ApJ, 654, 125
Shlosman I., Frank J., Begelman M. C., 1989, Nat, 338, 45
Shlosman I., Begelman M. C., Frank J., 1990, Nat, 345, 679
Shaerer D., Vacca W. D., 1998, ApJ, 497, 618
Shaerer D., Contini T., Kunth D., 1999, A&A, 341, 399
Sutherland R. S., Dopita M. A., 1993, ApJS, 88, 253
Tremonti C. A. et al., 2004, ApJ, 613, 898
Vacca W. D., Conti P. S., 1992, ApJ, 401, 543
van Albada G. D., Roberts W. W., 1981, ApJ, 246, 740
Veilleux S., Osterbrock D. E., 1987, ApJS, 63, 295 (V087)
Verdes-Montenegro L., Bosma A., Athanassoula E., 1995, A&A, 300, 65
Vila-Vilaró B. et al., 1995, A&A, 302, 58
Wada K., Habe A., 1992, MNRAS, 258, 82
Worthey G., 1994, ApJS, 95, 107
Worthey G., Ottaviani D. L., 1997, ApJS, 111, 377
Wozniak H., Friedli D., Martinet L., Martin P., Bratschi P., 1995, A&A, 111, 115
Zheng X. Z., Hammer F., Flores H., Assémat F., Rawat A., 2005, A&A, 435, 507

This paper has been typeset from a TEX/LATEX file prepared by the author.